



Cite this: *CrystEngComm*, 2021, **23**, 7928

Received 22nd February 2021,
Accepted 28th April 2021

DOI: 10.1039/d1ce00255d

rsc.li/crystengcomm

Transition metal oxide/hydroxide is intensively studied for the oxygen evolution reaction (OER). Herein, the graphene-induced growth of Co_3O_4 nanoplates with modulable oxygen vacancies via a hydrothermal treatment is reported. With the increase of reaction time before the formation of $\text{Co}(\text{OH})_2$, the oxygen vacancies and conductivity of Co_3O_4 nanoplates continued to increase resulting in dramatically enhanced OER performances. An ultralow overpotential of 354 mV at a current density of 100 mA cm^{-2} and a Tafel slope as low as $63.24 \text{ mV dec}^{-1}$ in 1 M KOH solution were obtained, superior to those of most reported oxides and RuO_2 .

Introduction

Owing to the depletion of fossil fuels and the increase of the greenhouse gases, energy conversion processes and storage devices, such as regenerative fuel cells, electrolysis cells, and metal-air batteries, have attracted great attention in the past decades.^{1–3} Among them, water splitting *via* photo electrocatalytic or electrocatalytic reaction is promising for producing reliable clean energy.^{4–6} The water splitting process consists of two parts: the hydrogen evolution reaction (HER) and the oxygen evolution reaction (OER). However, the OER often has a sluggish kinetics thus requiring high overpotentials, which will result in high energy consumption.^{5,7–11} One of the challenges is to develop excellent electrocatalysts using earth-abundant materials, with high stability and prominent catalytic activity. At present, noble-metal oxides (such as IrO_2 and RuO_2) are commercially used as OER catalysts, but their scarcity and high cost limit their applications. In recent decades, transition metal oxide/hydroxide has attracted great interests for the OER.

Transition metal-based compounds, such as sulfides, hydroxides, oxides, and phosphides, have been reported for the OER owing to their tunable electronic structures and abundant active sites. For example, Co_3O_4 , an inexpensive earth-abundant material, has been considered to be promising for the OER process because of its high electrical conductivity, adjustable structure, and oxygen defects.^{12–16} Generally, oxygen defects (such as oxygen vacancies and interstitials) are found to be vitally affecting the material properties such as electronic structure,¹⁷ conductivity,¹⁰ and intrinsic catalytic activity.^{18,19} Graphene has been intensively and extensively studied due to its excellent conductivity. It can also be used as a template to form two dimensional nanomaterials. Herein, we report the graphene-induced growth of Co_3O_4 nanoplates (denoted as $\text{g-}\text{Co}_3\text{O}_4$) *via* a hydrothermal treatment (HT) of pre-formed Co_3O_4 , where the oxygen vacancies are modulated by the reduction time until $\text{Co}(\text{OH})_2$ was formed. Note that graphene oxide was reduced during the hydrothermal process. Graphene assisted the formation of Co_3O_4 nanoplates, by contrast to the formation of bulky materials without graphene. The OER activity was evaluated over the as-obtained $\text{g-}\text{Co}_3\text{O}_4$ electrocatalysts. And oxygen defects and conductivity were analyzed with respect to the HT time.

Results and discussion

Fig. 1 shows the schematic diagram of the formation of $\text{g-}\text{Co}_3\text{O}_4$ nanoplates *via* a facile hydrothermal reaction. The morphology and particle size distribution diagram with respect to different reaction times were characterized by scanning electron microscopy (SEM). As shown in Fig. 2a and S1,[†] pristine Co_3O_4 has sphere-like morphology with an average size of 60 nm. The SEM images of $\text{g-}\text{Co}_3\text{O}_4$ are shown in Fig. 2b–e. The TEM image (Fig. S2[†]) of the home-made graphene shows clear wrinkles indicating an ultrathin film. When the HT time was 3 h, triangular nanoplates formed with an average lamellar size of *ca.* 0.17 μm and were uniformly coated by gauze-like graphene. Fig. 2c shows

^a The State Key Laboratory for Oxo Synthesis and Selective Oxidation, Suzhou Research Institute of LICP, Lanzhou Institute of Chemical Physics (LICP), Chinese Academy of Sciences, Lanzhou, 730000, China. E-mail: xinhengli@licp.ac.cn

^b University of Chinese Academy of Sciences, Beijing 100049, China

[†] Electronic supplementary information (ESI) available. See DOI: [10.1039/d1ce00255d](https://doi.org/10.1039/d1ce00255d)

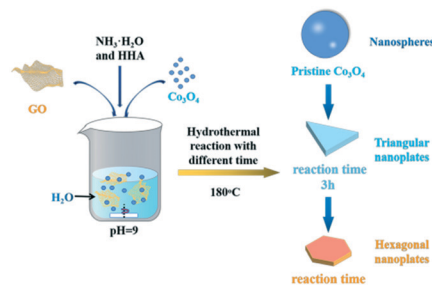


Fig. 1 Schematic illustration of the preparation of $\text{g-Co}_3\text{O}_4$ nanoplates via a hydrothermal treatment.

a further change of the material morphology as the reaction proceeded. Hexagonal nanoplates formed after 6 h, where graphene behaved like glue between the nanoplates. It can be clearly observed that the lamellar size increased fivefold to *ca.* 0.82 μm . After 6 h, the morphology of hexagonal nanoplates did not change much but its size gradually increased. As control experiments, the pristine Co_3O_4 samples were treated by the HT process without graphene, as shown in Fig. S3–S6,[†] which exhibited bulky materials instead of any nanoplate morphology. Therefore, we can come to a short conclusion that as a template, graphene assisted the formation of Co_3O_4 nanoplates.

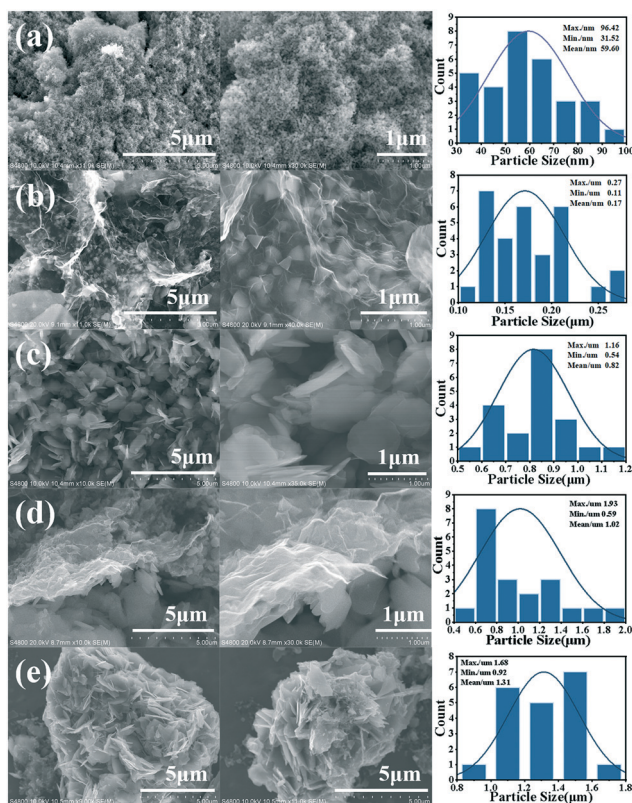


Fig. 2 SEM images and particle size distribution diagrams of pristine Co_3O_4 (a) and g-Co(OH)_2 with different hydrothermal reaction times: (b) 3 h; (c) 6 h; (d) 9 h and (e) 12 h.

The as-obtained samples of $\text{g-Co}_3\text{O}_4$ were characterized by XRD, as shown in Fig. 3a. The peaks at 19.00, 31.28, 36.88, 44.88, 55.68 and 59.38 and 65.28° can be attributed to the (111), (220), (311), (400), (422), (511) and (440) planes of Co_3O_4 (PDF no. 43-1003). It can be found that the pristine Co_3O_4 has a cubic crystal structure, and its cell parameters are: $a = b = c = 8.084$. As for $\text{g-Co}_3\text{O}_4$ 3 h and 6 h, it could be clearly observed that the characteristic peak intensity of Co_3O_4 decreased significantly. This proved that the crystal structure of the material had started to transition from a cubic structure of Co_3O_4 to a hexagonal structure of Co(OH)_2 . In other words, oxygen vacancies appeared in $\text{g-Co}_3\text{O}_4$ after 3 h due to reduction reaction. As for the sample of $\text{g-Co}_3\text{O}_4$ 12 h, the diffraction peak of the material is consistent with that of Co(OH)_2 with a hexagonal structure. And the cell parameters are $a = b = 3.183$, $c = 4.652$. So, $\text{g-Co}_3\text{O}_4$ 12 h is considered as Co(OH)_2 , and the remaining samples are Co_3O_4 with adjustable oxygen vacancies. Note that there is no obvious graphene signal in the catalyst, suggesting that the graphene content is very low. The existence of oxygen vacancies over the as-obtained samples were further confirmed by X-ray photoelectron spectroscopy (XPS). The pristine Co_3O_4 exhibits two subpeaks. The one at 529.8 eV corresponds to lattice O arising from the Co–O bond, and the other at 531.4 eV corresponds to oxygen vacancies. As the HT time increased until 9 h, the peak intensities and areas of the oxygen vacancies increased. From 9 h to 12 h, the formation of Co(OH)_2 made the oxygen defects disappear, corroborated by the Co 2p spectra as shown in Fig. S7.[†] The peaks at 779.8 eV and 781.3 eV for Co_3O_4 , $\text{g-Co}_3\text{O}_4$ 3 h and $\text{g-Co}_3\text{O}_4$ 6 h correspond to Co^{3+} and Co^{2+} , respectively. As the HT reaction time proceeded to 9 h and 12 h, only Co^{2+} was observed.

OER performances over pristine Co_3O_4 and $\text{g-Co}_3\text{O}_4$ were evaluated by cyclic voltammetry (CV) and linear sweep voltammetry (LSV). Fig. S8 and S9[†] show the CV curves of the $\text{g-Co}_3\text{O}_4$ and control experiments, as well as the LSV curves of the control experiments. It is proved that the active species was CoO(OH) . By contrast, the onset potential to form CoOOH decreased from 0.308 V to 0.272 V, and the overpotential decreased by 20 mV at a current density of 100 mA cm^{-2} over the $\text{g-Co}_3\text{O}_4$ 6 h electrocatalyst. Fig. 4 shows that the onset potentials to form CoOOH were only 0.256 V

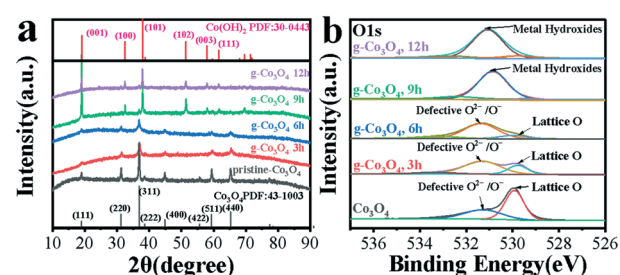


Fig. 3 (a) The XRD patterns and (b) O1s spectra of pristine Co_3O_4 (black) and $\text{g-Co}_3\text{O}_4$ with different hydrothermal reaction times: (red) 3 h; (blue) 6 h; (green) 9 h and (purple) 12 h.

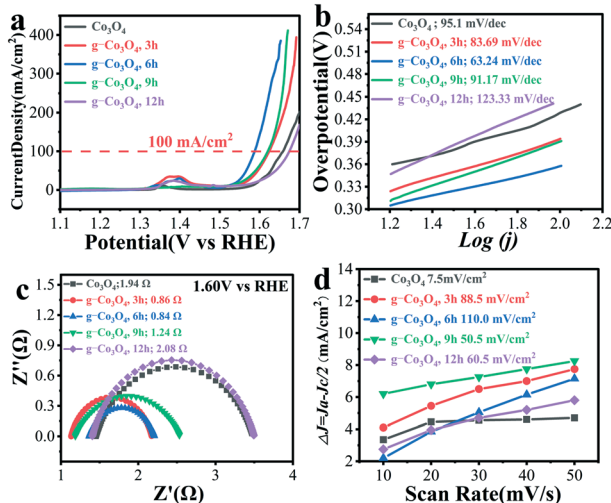


Fig. 4 (a) LSV curves of pristine Co_3O_4 (black) and g- Co_3O_4 with different hydrothermal reaction times: (red) 3 h; (blue) 6 h; (green) 9 h and (purple) 12 h. (b) Related Tafel slope. (c) and (d) Nyquist plots and double layer capacitance of the as-prepared catalysts.

and 0.239 V, respectively, over the g- Co_3O_4 3 h and g- Co_3O_4 6 h samples. And their overpotentials were 36 mV and 71 mV at 100 mA cm⁻², respectively, much lower than those over pristine Co_3O_4 , g- Co_3O_4 9 h and g- Co_3O_4 12 h.

The Tafel slope was employed to confirm the kinetic process of electron migration in the OER process. As shown in Fig. 4b, Co_3O_4 with a complete crystal structure exhibited a Tafel slope of 95.1 mV dec⁻¹. Electrochemical impedance spectroscopy (EIS) was then carried out to further probe the transfer kinetics of charge carriers (Fig. S9c† and Fig. 4c). Pristine Co_3O_4 show a small charge transfer resistance (R_{ct}) of 4.89 Ohm at a potential of 1.60 V vs. RHE. As the HT time increased, the R_{ct} significantly decreased. The as-prepared g- Co_3O_4 6 h exhibited an R_{ct} value as low as 0.84 Ω, corroborating the fast kinetics of water oxidation. The double-layer capacitance test further demonstrates that as the HT time increased, the electrochemical surface area (ECSA) increased. Combining with the above-mentioned results, we can conclude that the increase of oxygen vacancies and conductivity largely improved the catalytic activity.

Conclusions

In summary, the graphene-induced growth of Co_3O_4 nanoplates with modulable oxygen vacancies *via* a hydrothermal treatment was reported. With the increase of the hydrothermal reaction time before the formation of $\text{Co}(\text{OH})_2$, the oxygen vacancies and conductivity of Co_3O_4 increased, which resulted in greatly improved OER performances. An ultralow overpotential of 354 mV at a current density of 100 mA cm⁻² and a Tafel slope as low as 63.24 mV dec⁻¹ in 1 M KOH solution were obtained, superior to those of most reported oxides and RuO_2 . The enhanced activity can be attributed to the nanoplate morphology,

abundant oxygen vacancies and improved conductivity. Our strategy for the rational design of non-precious metal catalysts with superior OER activity can be applied to other systems, which may find ways for practical applications.

Conflicts of interest

There are no conflicts to declare.

Acknowledgements

This work was supported by the National Natural Science Foundation of China (21872157 and 21573263), the National Key Research and Development Program of China from Ministry of Science and Technology of China (2016YFE0105700), and the Natural Science Foundation of Jiangsu Province (BK20191198).

References

1. T. Chao, X. Luo, W. Chen, B. Jiang, J. Ge, Y. Lin, G. Wu, X. Wang, Y. Hu, Z. Zhuang, Y. Wu, X. Hong and Y. Li, *Angew. Chem., Int. Ed.*, 2017, **56**, 16047–16051.
2. C. C. McCrory, S. Jung, I. M. Ferrer, S. M. Chatman, J. C. Peters and T. F. Jaramillo, *J. Am. Chem. Soc.*, 2015, **137**, 4347–4357.
3. M. S. Dresselhaus and I. L. Thomas, *Nature*, 2001, **414**, 332–337.
4. E. Cui, G. Hou, X. Chen, M. Xie, F. Zhang, Y. Deng, Y. Wu and X. Yang, *Langmuir*, 2021, **37**, 894–907.
5. Q. Hu, X. Huang, Z. Wang, G. Li, Z. Han, H. Yang, P. Liao, X. Ren, Q. Zhang, J. Liu and C. He, *Small*, 2020, **16**, e2002210.
6. H. Yan, Y. Xie, A. Wu, Z. Cai, L. Wang, C. Tian, X. Zhang and H. Fu, *Adv. Mater.*, 2019, **31**, e1901174.
7. Z. Zhang, H. Zhang, Y. R. Yao, J. J. Wang, H. Guo, Y. D. Deng and X. P. Han, *ChemSusChem*, 2021, **14**, 1659–1673.
8. Z. H. Zang, X. W. Wang, X. Li, Q. L. Zhao, L. L. Li, X. J. Yang, X. F. Yu, X. H. Zhang and Z. M. Lu, *ACS Appl. Mater. Interfaces*, 2021, **13**, 9865–9874.
9. D. Wu, K. Kusada, S. Yoshioka, T. Yamamoto, T. Toriyama, S. Matsumura, Y. Chen, O. Seo, J. Kim, C. Song, S. Hiroi, O. Sakata, T. Ina, S. Kawaguchi, Y. Kubota, H. Kobayashi and H. Kitagawa, *Nat. Commun.*, 2021, **12**, 1145.
10. Z. Wei, W. C. Wang, W. L. Li, X. Q. Bai, J. F. Zhao, E. C. M. Tse, D. L. Phillips and Y. F. Zhu, *Angew. Chem., Int. Ed.*, 2021, **60**, 8236–8242.
11. P. Plate, C. Hohn, U. Bloeck, P. Bogdanoff, S. Fiechter, F. F. Abdi, R. van de Krol and A. C. Bronneberg, *ACS Appl. Mater. Interfaces*, 2021, **13**, 2428–2436.
12. N. F. Yu, W. Huang, K. L. Bao, H. Chen, K. Hu, Y. Zhang, Q. H. Huang, Y. Zhu and Y. P. Wu, *Dalton Trans.*, 2021, **50**, 2093–2101.
13. Y. Wu, Z. Xiao, Z. Jin, X. Li and Y. Chen, *J. Colloid Interface Sci.*, 2021, **590**, 321–329.
14. J. X. Flores-Lasluisa, F. Huerta, D. Cazorla-Amoros and E. Morallon, *Nanomaterials*, 2020, **10**, 22.

15 X. Yang, J. Chen, Y. Chen, P. Feng, H. Lai, J. Li and X. Luo, *Nano-Micro Lett.*, 2018, **10**, 15.

16 G. Zhang, J. Yang, H. Wang, H. Chen, J. Yang and F. Pan, *ACS Appl. Mater. Interfaces*, 2017, **9**, 16159–16167.

17 A. Karmakar, K. Karthick, S. Kumaravel, S. S. Sankar and S. Kundu, *Inorg. Chem.*, 2021, **60**, 2023–2036.

18 J. Dai, N. Shao, S. Zhang, Z. Zhao, Y. Long, S. Zhao, S. Li, C. Zhao, Z. Zhang and W. Liu, *ACS Appl. Mater. Interfaces*, 2021, **13**, 7259–7267.

19 H. Liu, H. Fu, Y. Liu, X. Chen, K. Yu and L. Wang, *Chemosphere*, 2021, **272**, 129534.